

Mechanisms of Summertime Subtropical Southern Indian Ocean Sea Surface Temperature Variability: On the Importance of Humidity Anomalies and the Meridional Advection of Water Vapor*

A. M. CHIODI AND D. E. HARRISON

Joint Institute for the Study of the Atmosphere and the Ocean, University of Washington, and NOAA/Pacific Marine Environmental Laboratory, Seattle, Washington

(Manuscript received 23 May 2006, in final form 29 January 2007)

ABSTRACT

It is well known that some austral summertime subtropical Indian Ocean sea surface temperature (SST) variability correlates with rainfall over certain regions of Africa that depend on rainfall for their economic well-being. Recent studies have determined that this SST variability is at least partially driven by latent heat flux variability, but the mechanism has not been fully described. Here, the mechanism that drives this SST variability is reexamined using analyses of operational air–sea fluxes, ocean mixed layer modeling, and simple atmospheric boundary layer physics. The SST variability of interest is confirmed to be mainly driven by latent heat flux variability, which is shown, for the first time, to be mainly caused by near-surface humidity variability. This humidity variability is then shown to be fundamentally driven by the anomalous meridional advection of water vapor. The meridional wind anomalies of interest are subsequently found to occur when the subtropical atmospheric anticyclone is preferentially located toward one of the sides (east/west) of the basin.

1. Introduction

In many South African countries, agricultural production depends largely upon summer rainfall, which is known to have levels of interannual variability that are a large fraction of the annual mean (see Mason and Jury 1997 for a review). Understanding rainfall variability in these regions is important because times of drought can adversely affect the economic well-being of tens of millions of people. Statistical methods have connected rainfall variability in many of these African countries with subtropical Indian Ocean SST anomalies. It has also been shown that prescribed Indian Ocean SST anomalies drive realistic rainfall anomalies in atmospheric models (Rocha and Simmonds 1997b; Reason and Mulenga 1999; Reason 2001; Goddard and

Graham 1999). This has led to a recent interest in determining the cause of these subtropical SST anomalies (cf. Behera and Yamagata 2001; Fauchereau et al. 2003; Suzuki et al. 2004; Hermes and Reason 2005). Latent heat variability, other components of surface heat flux, and ocean processes have all been implicated in forming these SST anomalies previously (Walker 1990; Yu and Rienecker 1999; Behera and Yamagata 2001; Suzuki et al. 2004; Hermes and Reason 2005), although the strongest case has been made for latent heat flux variability being the main cause of these subtropical SST anomalies.¹ Preliminary results, presented herein, confirm that latent heat flux variability is the main cause of these SST anomalies. This raises the question of what causes this latent heat flux variability. It has been suggested that modulations of the subtropical atmospheric anticyclone are responsible, although the link between atmospheric variability (i.e., anticyclone modulation) and SST variability has not been precisely

* PMEL Contribution Number 2927 and Joint Institute for the Study of the Atmosphere and the Ocean Contribution Number 1321.

Corresponding author address: A. M. Chiodi, NOAA/Pacific Marine Environmental Laboratory, 7600 Sand Point Way NE, Box 357941, Seattle, WA 98115.
E-mail: chiodi@ocean.washington.edu

¹ Hermes and Reason (2005) have also hypothesized that the geographical shape of the basin possibly favors the formation of dipolelike SST anomalies, although no evidence for a geography-based mechanism was given by these authors.

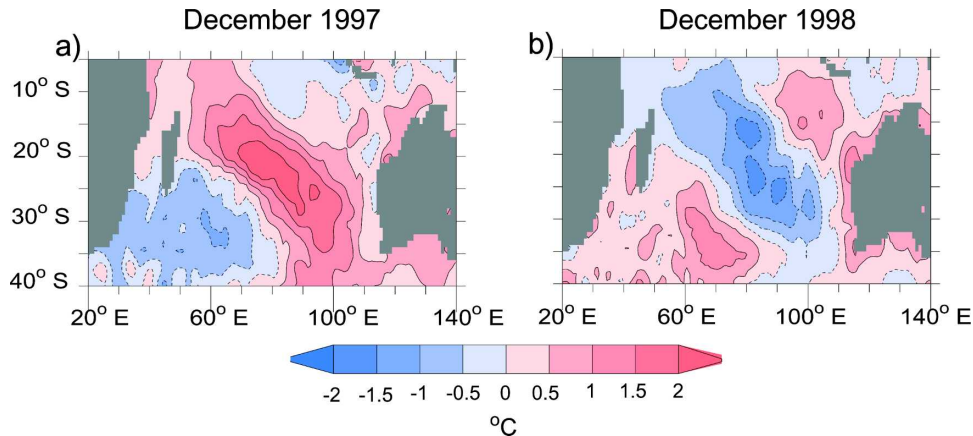


FIG. 1. December monthly mean SST anomaly (a) 1997 and (b) 1998. Reference period is 1990–2004. Data are from NOAA OISST.

determined. Investigations that have discussed the mechanism of these SST anomalies in detail have linked this latent heat flux variability to wind speed variability (e.g., Suzuki et al. 2004; Behera and Yamagata 2001). Here we reexamine the anomaly formation mechanism. Latent heat flux is parameterized in terms of two main variables [wind speed (S) and the surface (q_s) to near-surface (q_a) difference in specific humidity ($\Delta q = q_s - q_a$)], but the role of Δq anomalies has not been thoroughly investigated. It will be shown here that (i) Δq anomalies are usually the main cause of this latent heat variability, (ii) the Δq anomalies of interest are driven by the meridional advection of water vapor, (iii) the formation of the SST anomalies is characterized by abrupt austral summer warming that occurs when moist near-tropical air is advected southward along the western flank of the subtropical anticyclone, and (iv) the position of the subtropical atmospheric anticyclone largely determines the character of these SST anomalies.

SST variability in the subtropical southwestern Indian Ocean (the region south of Madagascar, 30°–45°S, 45°–75°E) is known to be positively correlated with rainfall in various regions of southern Africa (cf. Walker 1990; Rocha and Simmonds 1997b; Reason and Mulenga 1999; Reason 1999; Goddard and Graham 1999; Behera and Yamagata 2001). SST nearer the center of the subtropical basin has been shown to be inversely correlated with rainfall in these same regions of Africa. Furthermore, SST anomaly patterns that have an anomaly of one sign in the southwest and another sign midbasin (e.g., Fig. 1) are seen in spring and early summer of individual years (Reason 1999; Hermes and Reason 2005) and are present in statistical decompositions of SST data (Behera and Yamagata 2001; Fauchereau et al. 2003). Recent work has determined

that the cooling and warming tends to happen simultaneously (Suzuki et al. 2004; Hermes and Reason 2005).

Warm (cool) SST anomalies have tended to occur in the southwestern (midbasin) subtropics in the austral spring to early summer of La Niña years, and the opposite pattern has tended to occur during spring/summer of El Niño years. Both types of anomalies, however, can be seen in years which are neither El Niño nor La Niña (cf. Nicholson 1997; Reason 1999; Behera and Yamagata 2001). The rainfall–SST correlation is present even when El Niño and La Niña years are deleted from the datasets (Rocha and Simmonds 1997a; Walker 1990).

Some recently described tropical Indian Ocean variability has been found to have a roughly similar relationship to El Niño–Southern Oscillation (ENSO) variability (Huang and Kinter 2002; Saji and Yamagata 2003) as the subtropical SST variability discussed here. Important aspects of this tropical Indian Ocean SST variability have been shown to be driven by remotely forced ocean dynamics, such as equatorial Rossby waves [see Xie et al. (2002) and Behera et al. (2000), for comparison; experiments showing the purely 1D ocean response to ENSO-related atmospheric variability can be found in Alexander et al. (2002)]. Although the formation mechanism of the subtropical SST anomalies discussed here (described below) is different than many of those that have been shown to be prevalent in the Tropics (e.g., Xie et al. 2002), the tendency for each to coincide with ENSO variability suggests that both may be ultimately driven by coupled air–sea interaction.

Tripolar interannual SST anomalies, roughly similar in pattern to the ones described here, have been discussed recently by England et al. (2006). In this case, the SST anomalies were found using the National Oceanic and Atmospheric Administration (NOAA) Ex-

tended Reconstructed SST composites based on annual rainfall extremes in southwest Western Australia. These SST anomalies were found to have an annual time scale and magnitudes up to 0.5°C . They were found to be driven by a variety of geographically dependent processes, including Ekman advection and surface heat flux variability. Meridional wind variability was found to be important to some of the surface heat flux variability described by England et al., although the mechanism responsible was not discussed in detail.

An example of the SST anomaly pattern examined here can be seen in the summer months of November 1998 through February 1999, when warm SST anomalies (0.5° – 1.5°C) were observed south and southeast of Madagascar (e.g., Fig. 1b). A negative SST anomaly of similar magnitude, stretching from approximately 15°S , 50°E to 30°S , 100°E was also observed at this time. The northwest to southeast slant of this midbasin anomaly is a typical characteristic of these SST anomalies. The opposite pattern of warm midbasin–cool southwestern anomaly was observed in the summer of 1997/98 (e.g., Fig. 1a). In this case, the midbasin positive anomaly exceeded 2°C .

We focus our analysis on the processes at work in late spring to early summer. This time of year was chosen because the link between SST and rainfall is known to be strongest at this time and also because the SST anomalies in question have been shown to depend primarily upon late spring to early summer heat flux anomalies. Two recent years in which the SST pattern in question was observed are used as case examples. Composites, formed by averaging data from many different years, are also used to check the robustness of the case study results.

It will be shown that the mechanism discussed here applies to a range of time scales (biweekly to seasonal or longer). Although the phenomena discussed here have traditionally been considered on a seasonal or longer time scale, phenomena are mainly examined here at biweekly or monthly resolution. This time scale is used because many details of the atmospheric variability discussed here are comparatively obscured by averaging over a season or longer.

This paper is organized as follows. Section 2 describes the data and ocean mixed layer model used herein. Section 3 describes ocean model case study experiments. Section 4 examines Δq , S , and latent heat variability from a numerical weather prediction model. Section 5 discusses the prevalent atmospheric phenomena and identifies a relevant sea level pressure (SLP) index. Section 6 delineates the temporal variability of this SLP index. Section 7 more thoroughly examines

the anomaly formation mechanism. Section 8 provides a summary and discussion.

2. Data and ocean mixed layer model

Daily mean net surface heat fluxes, momentum fluxes, and precipitation were obtained from the National Centers for Environmental Prediction (NCEP) reanalysis project (available online at <http://www.cdc.noaa.gov>). The NCEP fluxes are estimated on a Gaussian grid (approximately $2^{\circ} \times 2^{\circ}$) from a global atmospheric model supplied with conventional as well as satellite-based data (Kalnay et al. 1996). The fluxes are not generally measured by conventional methods and may be thought of as model estimates that are constrained by data supplied to the model. The components of 10-m wind (\mathbf{V}), 2-m q_a , and surface skin temperature were also obtained from the NCEP reanalysis. Surface humidity was estimated with skin temperature, assuming that the surface is saturated.

The variable Δq from the NCEP model depends upon the modeled values of q_a , which are not generally constrained by observations and thus may contain errors due to imperfections in the model. Smith et al. (2001) found that, at 6-h resolution, the root-mean-square (rms) difference between q_a from high-quality in situ measurements (World Ocean Circulation Experiment, 1990–95) and from the NCEP reanalysis was 1.3 g kg^{-1} . The NCEP reanalysis also showed an average warm bias that was on the order of 0.1 g kg^{-1} . Given climatological subtropical bulk flux parameters (e.g., 1.2 kg m^{-3} air density; 6 m s^{-1} wind speed) the 1.3 g kg^{-1} error in q_a reported by Smith would account for a random error of about 30 W m^{-2} in the 6-hourly latent heat flux. This rms difference should be reduced 10-fold in the monthly mean averages discussed here because roughly 120 6-h samples are averaged per month. The latent heat flux anomalies discussed below are about twice as large as the 30 W m^{-2} error associated with Smith's description of 6-hourly q_a error. Thus at monthly time scales, the signal-to-noise ratio is favorable for the analysis described herein.

NOAA optimally interpolated SST (OISST) was obtained from the NOAA Climate Diagnostics Center (available online at <http://www.cdc.noaa.gov>). OISST is a weekly dataset that merges in situ and satellite-based SST observations (Reynolds et al. 2002).

For comparison purposes, SST was reproduced by integrating the surface flux fields in an ocean mixed layer model (Price et al. 1986). The model used here was configured to resolve the upper 500 m of the water column. Initial conditions were taken from the Levitus (1994) climatology. This model deepens the mixed

layer (thereby entraining deeper water) when vertical shear exceeds a critical bulk Richardson number (0.65) or when static instability occurs. Stratification is restored based on buoyancy input from freshwater or a net flux of heat into the ocean. Penetrative shortwave radiation is assumed to consist of two components, absorbed with 0.6- and 20-m *e*-folding scales, respectively (Paulson and Simpson 1977). All other surface fluxes are applied entirely to the mixed layer. Integrations are performed with vertical resolution set at 1 m in order to well resolve shallow summertime mixed layer depths. A background diffusion of $2 \times 10^{-5} \text{ m}^2 \text{ s}^{-1}$ is applied uniformly throughout the water column. The diffusion acts to lower unreasonably high SSTs, which may occur in the model when very thin mixed layers develop during summer. The diffusion may be thought of as a crude stand in for unresolved processes, such as internal wave breaking. Integrations begin in the austral winter and are carried out through summer. Experiments have shown that the results presented here are not sensitive to initial conditions, so long as the starting temperature profile is reasonable, for example, the mixed layer is deep to begin with and the mixed layer temperature is within several degrees of observed SST.

The effects of surface currents on SST tendency were examined using currents from the Simple Ocean Data Assimilation (SODA; available online at <http://www.atmos.umd.edu>). Currents from SODA were used for this purpose because, unlike currents from the mixed layer model described above, they contain geostrophic components (Carton et al. 2000).

3. Ocean mixed layer model results

To test whether surface fluxes drive the SST anomalies of interest here, and whether the processes that cause this surface flux variability are well resolved in the NCEP reanalysis, we have compared observed temperature tendencies with tendencies predicted from an ocean mixed layer model forced with NCEP surface fluxes. Case studies of two recent examples are described here.

Observations show that the warm SST anomalies seen in December of 1997 and 1998 (Fig. 1) are largely driven by changes in SST that occur in November of 1997 and 1998, respectively. These SST changes are characterized by abrupt warming in specific coherent regions that cover much (2500 km) but not all of the basin. These warming regions appear in a different location in each case. For example, abrupt warming of SST (2° – 4°C) was observed in the central subtropics (centered around 20°S , 75°E) during November of 1997 (Fig. 2a). Similarly, abrupt warming was also observed

during November of 1998, although, in this case, the 2° – 4°C warming was seen in the southwestern subtropics (centered around 35°S , 55°E in Fig. 2b). Monthly warming of the same large spatial scale and magnitude was not observed in either October 1997 or October 1998 (not shown).²

The observation of abrupt November SST warming that is roughly collocated with warm December SST anomalies supports the findings of Suzuki et al. (2004) who claim that these anomalies form in late spring to early summer because the ocean mixed layer depth is shallow then, making SST highly sensitive to surface heat flux anomalies.

Many aspects of the observed SST tendencies are reproduced in the ocean mixed layer model. Most importantly, coherent regions that warm abruptly and have similar shape, location, and amplitude as observations are clearly seen in model SST. In 1997, for example, the shape and magnitude of the coherent, abrupt warming region seen in the observations (20°S , 70°E) is reasonably well reproduced by the model (Fig. 2c). SST increases by $>2^{\circ}\text{C}$ during November 1997 in the regions east of Madagascar (22°S , 60°E) and west of Australia (25°S , 93°E) in the model, as it does in observations. Some discrepancies are apparent between the model and the observations. In 1997, for example, the warming tendency is overpredicted at 22°S , 60°E and underpredicted at 25°S , 85°E . These discrepancies may be caused by errors in the fluxes or model physics. Despite these possible sources of error, the overall temperature tendency predicted by the model correlates well with observations (spatial correlation is 0.78 for November 1997 and 0.72 for November 1998 in the region 10° – 40°S and 20° – 140°E). Note that in the southwestern subtropics (33°S , 50°E) warming of less than 0.5°C or cooling is seen in both the model and observations during November 1997, whereas during November 1998, both model and observations show warming of $>2^{\circ}$ in this location. Also note that during November 1998, neither the observations nor model show warming $>1^{\circ}$ in the central subtropical region that was observed to warm abruptly during November 1997. The fidelity of the model results discussed here strongly suggests that the SST anomalies in question are driven by surface fluxes of heat and/or momentum.

Surface momentum flux anomalies can drive SST anomalies by causing entrainment of water below the

² Localized warming of 2° – 3°C was observed at 34°S , 85°E during October 1997, but this warming was smaller in spatial scale and magnitude than the warming seen in November. No southern subtropical Indian Ocean region was observed to warm by more than 2°C during October 1998.

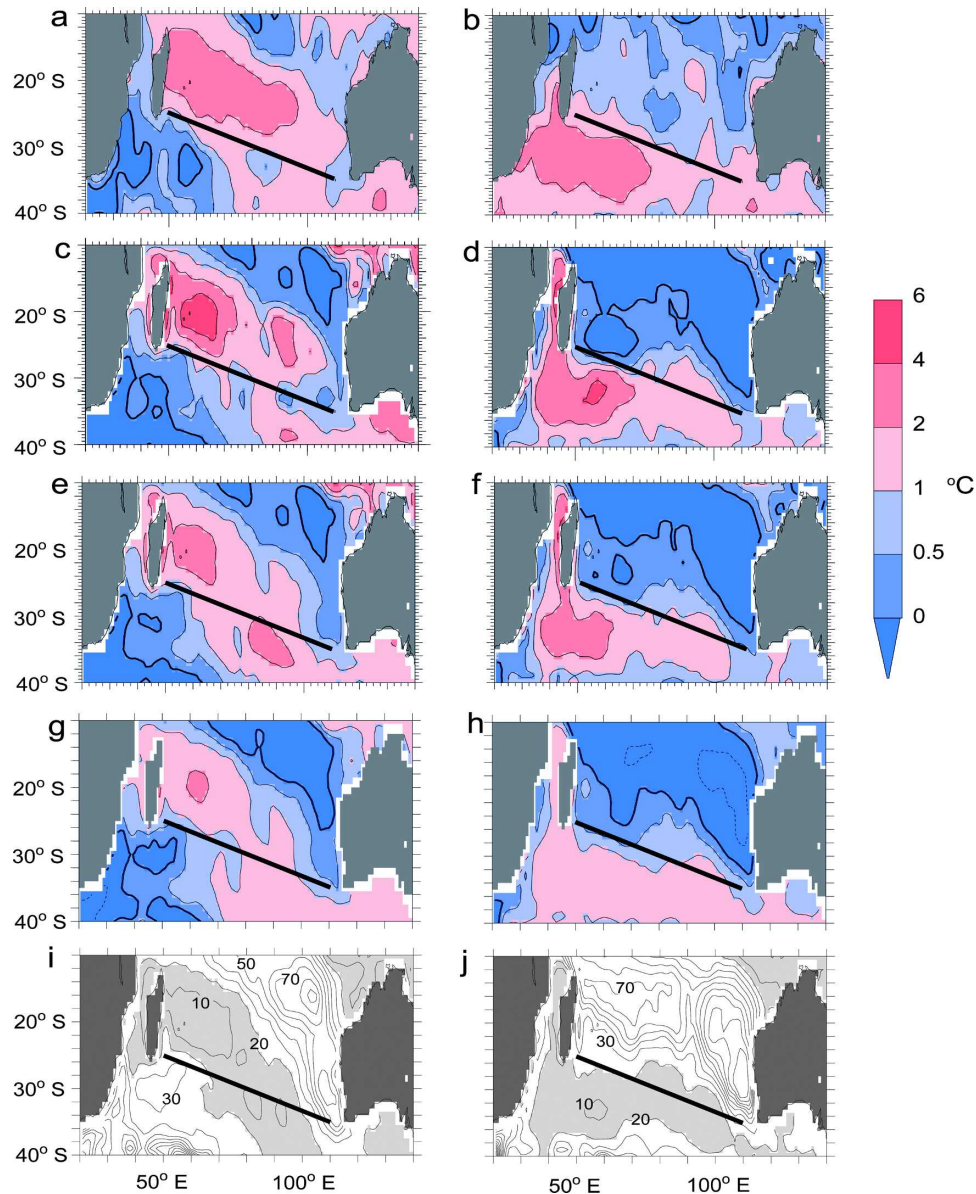


FIG. 2. Observed temperature change between 1–30 Nov (a) 1997 (b) 1998. (c) As in (a), except the temperature change is estimated by an ocean mixed layer model using NCEP surface fluxes. (d) As in (c), except for 1998. (e) As in (c), except the climatological monthly mean momentum flux, rather than the daily mean momentum flux is used. (f) As in (e), except for 1998. (g) Model run similarly to (c), except that the mixed layer depth is fixed at 35 m. (h) As in (g), except for 1998. (i) Mean November 1997 model mixed layer depth. Contour interval is 10 m. Depths less than 20 m are shaded light gray. (j) As in (i), except for 1998. The straight black line is drawn to roughly mark the division between the observed anomalous warming and cooling regions.

mixed layer and/or by affecting the mixed layer depth, which controls the sensitivity of SST to surface heat flux anomalies. The model experiments described below show that, although momentum anomalies contribute to the SST anomalies discussed here, these SST anomalies are not fundamentally caused by momentum anomalies. When momentum anomalies are removed

from the forcing—by using climatological monthly mean wind stress (period 1992–2004) rather than daily mean wind stress—the shape and amplitude of the SST anomalies change by a relatively small amount. In the 1998 case, the average warming amplitude in the southwestern subtropics changes by only about 10% (Fig. 2f). In 1997, wind stress variability has slightly

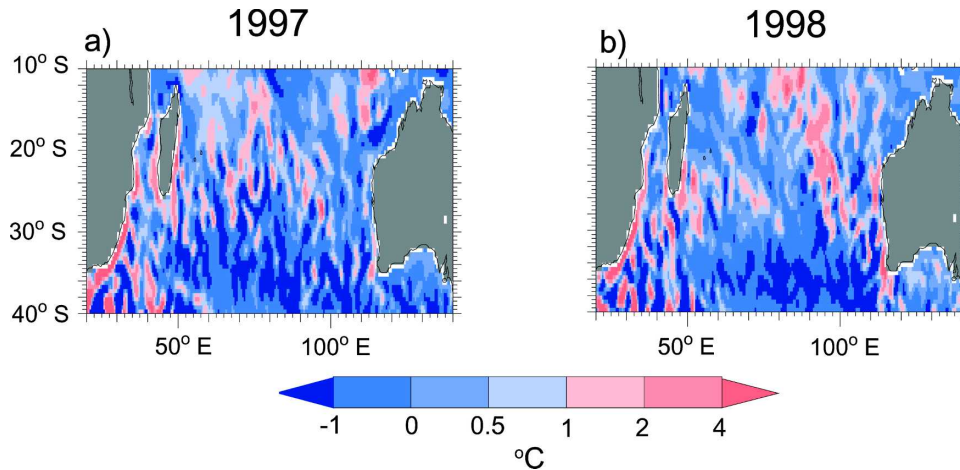


FIG. 3. Estimated temperature tendency (change from 1–30 Nov) due to SODA surface currents during November (a) 1997 and (b) 1998.

more effect on the modeled temperature tendency (Fig. 2e). Most notably, warming at 35°S, 90°E is enhanced while warming at 25°S, 93°E is diminished. The general pattern of low warming to cooling in the southwest and abrupt warming in the central basin, however, is preserved in the 1997 run that excludes wind stress variability. The results of these model experiments show that heat flux anomalies mainly drive the temperature tendencies seen in the model. This result is consistent with previous studies of the effects of wind stress and heat flux variability on tropical/subtropical Atlantic (Carton et al. 1996) and Indian Oceans (Behera et al. 2000) SST variability.

It is notable that the warming tendencies discussed above are significantly larger than the cooling tendencies. This occurs even though the positive and negative surface heat flux anomalies that drive these tendencies have similar magnitudes (as described below). Model results suggest that warming tendencies are larger partly because the ocean mixed layer tends to shoal in response to incoming heat flux anomalies. Thus, incoming heat anomalies are spread over a thinner mixed layer and thereby produce larger changes in SST. This can be seen by comparing the mixed layer depth estimated by the model in each case. Averaged over 1997, for example, the model mixed layer depth is less than 20 m deep throughout much of the central basin region and deeper than 30 m in much of the southwestern basin (Fig. 2i). In the 1998 case, however, the model mixed layer is considerably deeper than 30 m in much of the central basin region and less than 20 m deep in the majority of the southwestern basin (Fig. 2j). Correspondingly, peak warming is reduced by factors of 2–3 in the runs with mixed layer depths held fixed at 35 m (roughly the model average for November).

The effects of ocean surface currents during November 1997 and 1998 have been estimated but found to play a secondary role, at best, in the formation of the SST anomalies discussed here. The advective temperature tendency is found by integrating surface temperature advection (currents from SODA; SST gradients from NOAA OISST) from 1 to 30 November. In either case, the advective temperature tendencies (Figs. 3a,b) do not appear to have the same coherent patterns that appear in the observed net SST tendencies (Figs. 2a,b). Currents from the ocean mixed layer model runs were also used to estimate the advective temperature tendencies (computed as per Price et al. 1986). These tendencies also were found to lack the patterns necessary to drive the observed SST anomalies and are not shown for brevity.

A comparison of the heat flux anomalies estimated by the NCEP reanalysis quickly reveals that only latent heat flux anomalies have the magnitude and pattern necessary to drive the observed SST anomalies (Fig. 4; see also Behera and Yamagata 2001; Suzuki et al. 2004; Hermes and Reason 2005). In 1997, a pattern commensurate to the warm central basin–cool southwestern basin December 1997 SST anomaly was apparent in the November NCEP latent heat flux anomaly; the November 1997 latent heat flux anomaly has a midbasin minimum (40–80 W m^{-2}) centered at 20°S, 65°E that extends toward the southeast, such that low anomalies of 20–40 W m^{-2} are seen throughout most of the central Indian Ocean, between 20° and 28°S (Fig. 4a). A maximum in latent heat loss (20–60 W m^{-2}) is also apparent in the southwestern subtropics (30°S, 50°E) in 1997. Thus, by NCEP estimates, the oceanic region east of Madagascar gained up to 80 W m^{-2} more than usual in November 1997, while the southwestern subtropics lost

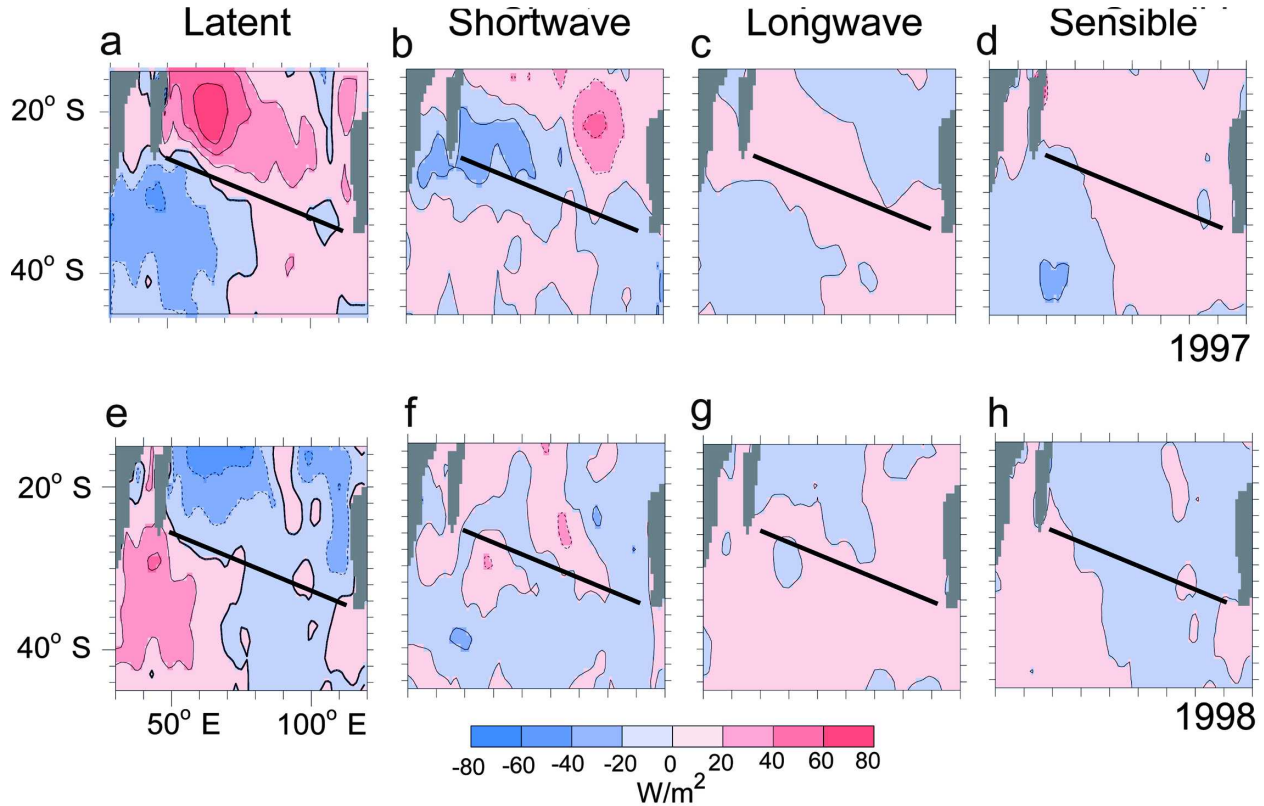


FIG. 4. Average net surface anomaly values for 1–30 Nov 1997: (a) latent heat flux, (b) shortwave radiation, (c) longwave radiation, and (d) sensible heat flux. (e)–(h) are the same as (a)–(d), except for 1998. Downward anomalies are positive. The straight black line roughly marks the division between regions of observed anomalous warming and cooling (see Fig. 2).

up to 60 W m^{-2} more than the monthly climatological average. The latent heat flux anomaly that appears in November of 1998, in many regards, is opposite that of November 1997 (Fig. 4e). Again, a dipole pattern is apparent between the southwest and central subtropics in 1998, but the pattern is reversed with respect to 1997 so that $40\text{--}80 \text{ W m}^{-2}$ less heat than usual is lost over most of the southwest and $20\text{--}60 \text{ W m}^{-2}$ more is lost in the central subtropics. Note that the magnitudes of the sensible and longwave heat flux anomalies are much smaller than the latent heat flux anomaly and therefore play secondary roles in creating SST anomalies (Figs. 4c,d,g,h). Note also that the patterns seen in the shortwave anomalies do not have the shape needed to drive the SST anomalies discussed here (Figs. 4b,f).

In summary, observations indicate that abrupt warming occurs in November, leading up to the warm anomalies observed in December. Mixed layer model integrations of NCEP-derived heat fluxes reproduce the location and general magnitude of this warming, and only latent heat flux anomalies are of appropriate magnitude and pattern to drive the SST anomalies in question.

4. The relationship between Δq , S , and latent heat flux variability in the NCEP reanalysis

In this section we compare the relative effects of wind speed and Δq anomalies on latent heat flux. First, a formal relationship is found from a simple perturbation analysis of the bulk parameterization of latent heat flux (e.g., Large and Pond 1981):

$$Q_{\text{LH}} = C_e L_e \rho S \Delta q, \quad (1)$$

where C_e is the exchange coefficient, L_e is the latent heat of vaporization, and ρ is air density. It is straightforward to find that

$$\frac{Q'_{\text{LH}}}{\overline{Q_{\text{LH}}}} \approx \frac{\Delta q'}{\overline{\Delta q}} + \frac{S'}{\overline{S}} \quad (2)$$

(appendix A). Here, Q'_{LH} is the monthly latent heat anomaly with respect to the monthly mean climatology $\overline{Q_{\text{LH}}}$ (with similar notation for S and Δq).

For the remainder of the paper, we will use the absolute value of the ratio

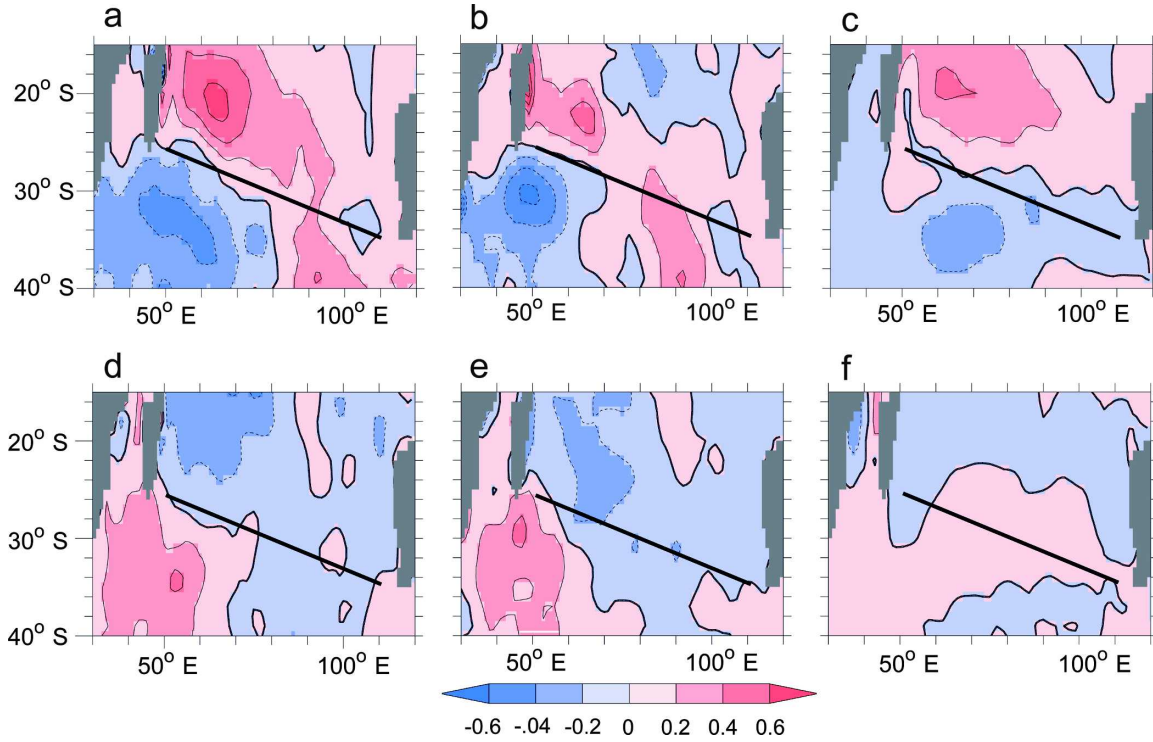


FIG. 5. November 1997 mean (a) r_{LH} , (b) $r_{\Delta q}$, and (c) r_s . (d)–(f) As in (a)–(c), except for 1998. Anomalies that would tend to cause anomalous warming of SST are positive (red). The straight black line roughly marks the division between regions of observed anomalous warming and cooling (see Fig. 2).

$$R = \frac{\frac{\Delta q'}{\overline{\Delta q}}}{\frac{S'}{\overline{S}}} \quad (3)$$

to determine the primacy of these terms. Since the variables in Eq. (2) are all readily available from the NCEP reanalysis, this method provides a quantitative measure of the relative importance of $\Delta q'$ and S' to Q'_{LH} . To be more concise hereafter, we define

$$r_{LH} \equiv \frac{Q'_{LH}}{Q_{LH}}, \quad (4)$$

$$r_s \equiv \frac{S'}{\overline{S}}, \quad \text{and} \quad (5)$$

$$r_{\Delta q} \equiv \frac{\Delta q'}{\overline{\Delta q}}. \quad (6)$$

Consider the dipolelike pattern apparent in the November 1997 NCEP latent heat flux anomaly (Fig. 4a). Equation (2) tells us that a commensurate dipolelike pattern must be present in either $r_{\Delta q}$, r_s , or their sum. Such a pattern is clearly seen in the November 1997 Δq anomaly (Fig. 5b). A maximum and minimum appear in $r_{\Delta q}$ at roughly the same locations as the previously men-

tioned latent heat extrema. Furthermore, Δq in the southwestern subtropics is 20%–60% less than the climatological monthly mean. This same dipole pattern is not so apparent in the November 1997 S anomaly (Fig. 5c). Although an S minimum (40%–60% lower than normal) appears at roughly the same location as the midbasin latent heat flux minimum (20°S, 60°E), a slight local S minimum (0%–20%) is also shown in the southwestern subtropics (30°S, 50°E), which obviously counters some of the effect of the southwestern subtropical Δq anomaly. In this case, the southwestern latent heat flux anomaly is mainly due to Δq variability and the midbasin anomaly depends on both S and Δq variability.

The latent heat anomaly apparent in November 1998 clearly appears to be driven by Δq variability. Similarly to r_{LH} , $r_{\Delta q}$, abruptly changes sign moving from the southwestern subtropics to the region east of Madagascar. Minimums in both heat loss and Δq are centered near 30°S, 48°E. As estimated by the NCEP reanalysis, Δq was 40%–60% lower than average over most of the southwestern subtropics during November 1998 and 0%–40% larger than normal over much of the central subtropics. As in 1997, both the latent heat flux and Δq anomaly patterns have a similar northwest to southeast orientation, whereas the wind speed anomaly is ori-

TABLE 1. (first row) Spatial correlation of $r_{\Delta q}$ and r_{LH} in the Indian Ocean, 15° to 45°S. (second row) As in first row, except for r_s . (third row) Mean difference between the highest and lowest 5% of $r_{\Delta q}$ values in the Indian Ocean. (fourth row) As in third row, except for r_s .

	1993	1994	1995	1996	1997	1998	1999	2000	2001	2002	2003
$r_{\Delta q}-r_{LH}$ correlation	0.50	0.71	0.72	0.70	0.77	0.85	0.63	0.69	0.48	0.82	0.69
r_s-r_{LH} correlation	0.41	0.25	0.54	0.38	0.61	0.55	0.53	0.61	0.49	0.61	0.54
$r_{\Delta q}$ range	0.57	0.76	0.64	0.58	1.0	0.71	0.67	0.70	0.64	0.88	0.58
r_s range	0.27	0.30	0.31	0.27	0.50	0.26	0.33	0.36	0.38	0.33	0.32

ented zonally. The pattern seen in r_s has a smaller range of values than $r_{\Delta q}$; the vast majority of the wind speed anomalies are within 20% of the climatological mean.

Averaged over the region considered, there is quantitative evidence that $\Delta q'$ is more important than S' . The spatial correlations between $r_{\Delta q}$ and r_{LH} (0.77, 0.85) are higher than for r_s and r_{LH} (0.61, 0.55) in both 1997 and 1998. The range of the $r_{\Delta q}$ is also larger than the range of r_s (Table 1). In general, the magnitude of r_s is 0.4 or lower, while both r_{LH} and $r_{\Delta q}$ reach levels of 0.8 or higher. This means that the large latent heat anomalies described here (up to 80 W m^{-2}) would be unlikely to occur if wind speed were the only factor contributing to latent heat flux variability. Only two years are discussed here in detail for brevity, but analysis has shown that, compared to r_s , $r_{\Delta q}$ has a larger range and is more highly correlated with r_{LH} for all but one year (2001) between 1993 and 2003 (Table 1).

5. Atmospheric variability

This section describes the atmospheric phenomena that create the latent heat flux anomalies described above. Visual inspection of SLP and near-surface wind fields suggest that conditions favorable to warming are created within the central/western flank of the subtropi-

cal atmospheric anticyclone; November 1998 monthly mean winds clearly show that the anticyclone is adjacent to the region of rapidly warming SST (Fig. 6b). Furthermore, November 1997 monthly mean winds show a clear shift of the anticyclone to the east (see Fig. 6a), consistent with the warming observed then. To test whether anticyclone position determines the location of the abrupt warming, we have defined a simple index for anticyclone position and asked whether or not it might be used as a proxy for the observed latent heat flux and SST anomaly patterns.

This index is based on the difference of daily mean NCEP SLP anomaly between the approximate position of the November 1998 SLP high ($37^\circ\text{--}28^\circ\text{S}$, $60^\circ\text{--}70^\circ\text{E}$) and the November 1997 SLP high ($37^\circ\text{--}28^\circ\text{S}$, $85^\circ\text{--}100^\circ\text{E}$). This difference is smoothed with a 15-day boxcar filter and resampled every 15 days, starting 1 January 1992, resulting in approximately 150 values. The November through March values were sorted and the 25 largest and smallest were chosen to form composites of the low-level atmosphere. Fifteen-day averages, bracketing each of these extrema, were first calculated from daily averages of the relevant atmospheric variables. Then, the averages from each group of 25 days were combined to form two composites representing the average atmospheric conditions during times in

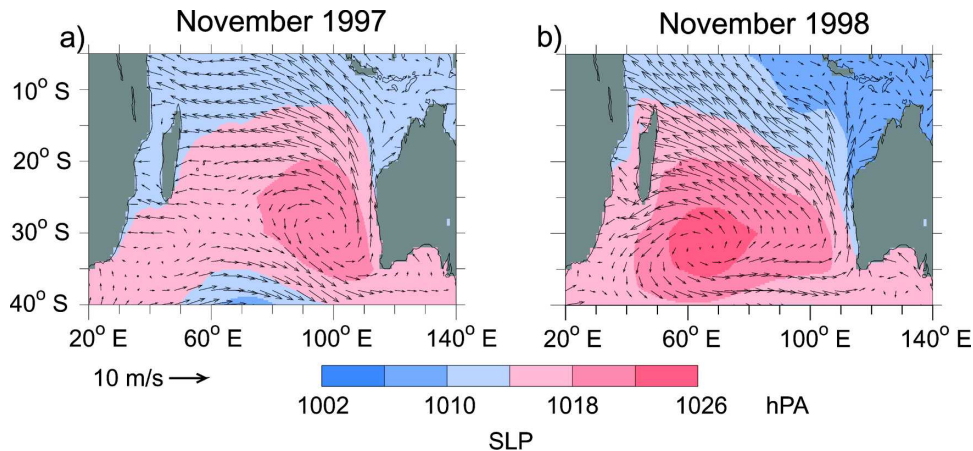


FIG. 6. November mean SLP (color field) and 10-m winds (vectors): (a) 1997 and (b) 1998.

which the west to east SLP difference was anomalously large and small, respectively.

The high western SLP composite (Fig. 7a) clearly shows the anticyclone positioned to the west, similar to the November 1998 average conditions. Likewise, the high eastern SLP composite (Fig. 7b) shows the anticyclone positioned to the east, as in the November 1997 average. The difference of the two latent heat flux composites bears a close resemblance to the anomalies seen in 1997 and 1998 (Fig. 7c). The composite difference pattern clearly changes sign moving from the southwestern basin to the region east of Madagascar, similarly to the SST anomaly pattern in question. The poles of these SLP and latent heat flux anomalies are significant at the 90% confidence level (Figs. 7d–f; Student's t method; the composite difference is shown only where both composite anomalies are significantly different from the mean).

Compositing further suggests that the meridional advection of water vapor mainly causes the latent heat flux/SST anomaly pattern discussed here since this pattern is also apparent in composite differences of meridional wind, humidity advection ($-\mathbf{V} \cdot \nabla_h q_a$), and SST anomalies (Figs. 7g–i, time indices are lagged 1 week for SST). For each of these variables, the anomalies that are centered in the southwestern and central basin regions are significant at the 90% confidence level. The relationship among these variables will be examined further in section 7.

6. Indices of atmosphere–ocean interaction

The observed interannual variability of SST compares favorably with the SLP-based index described above. For comparison purposes, an SST anomaly index was formed by differencing two 30-day mean SST anomalies; one averaged within the southwestern region (40° – 30° S, 45° – 65° E) and the other averaged within the central basin region (25° – 15° S, 60° – 80° E). These regions are similar to those used previously (e.g., Hermes and Reason 2005; Behera and Yamagata 2001) to index southern subtropical Indian Ocean SST variability (a comparison is given below). This index is significantly correlated with the average November SLP index described above (Fig. 8a; 0.66 correlation; 95% confidence level is 0.57; Fisher's z with 12 degrees of freedom). There are some discrepancies between the SLP and SST index. For instance, large negative SLP index values do not always correspond to large negative SST index values (e.g., year 2003). Such discrepancies may reflect the inability of this simple SLP index to adequately represent all atmospheric variability. This is suggested by the higher correlations found between the

SST index and the other three indices described above (0.90, 0.83, and 0.73 for latent heat, meridional wind, and $-\mathbf{V} \cdot \nabla q_a$, respectively). Discrepancies may also be due to errors in the surface fluxes or secondary sources of SST variability; however, the reasonable agreement between each of these indices suggests that the SST variability is driven by latent heat flux/meridional advection anomalies.

Results have shown that the methodology used here remains valid on seasonal time scales. For example, we have repeated the above analysis by comparing the atmospheric conditions during the seasonal onset of these anomalies (November through March) with the SST anomalies in the peak (February and March) season (this timing was originally proposed by Hermes and Reason 2005). When averaged over these times, the SLP index described above remains highly correlated to the latent heat flux, meridional wind, $-\mathbf{V} \cdot \nabla q_a$, and SST indices (0.86, 0.50, 0.89, and 0.75 correlations, respectively; 95% confidence level = 0.57). This suggests that the interannual variability of these SST anomalies depends fundamentally on the mechanism discussed here.

Because these SST anomalies peak in somewhat different locations each year, a unique spatial definition is unlikely to capture each peak (Hermes and Reason 2005). Accordingly, the regions used for the SST index described above (based on the November 1997 and November 1998 case examples) are somewhat different than those described by Hermes and Reason (44° – 30° S, 44° – 74° E and 35° – 19° S, 80° E:110°E) and by Behera and Yamagata (2001) (37° – 27° S, 55° – 65° E, 28° – 18° S, 90° – 100° E). Each of these indices, however, show very similar variability over the period examined here (Fig. 8c; all cross correlations are above 0.82).

7. The relationship between Δq , S , and latent heat flux in an idealized atmospheric mixed layer

In this section we examine the formation mechanism of these anomalies more closely. A simple scale analysis suggests that humidity advection ($-\mathbf{V} \cdot \nabla_h q_a$) can easily change Δq in the subtropics. The relevant horizontal length scale

$$l = \frac{\Delta q}{|\nabla_h q_a|} \quad (7)$$

is near 1000 km in the subtropics and smaller at higher latitudes (Fig. 9). Contours of q_a closely follow contours of SST. Thus, $\nabla_h q_a$ points mainly in a northward direction and $\mathbf{V} \cdot \nabla_h q_a$ is dominated by the meridional term. This means that meridional advection associated with synoptic-scale atmospheric phenomena (length scales

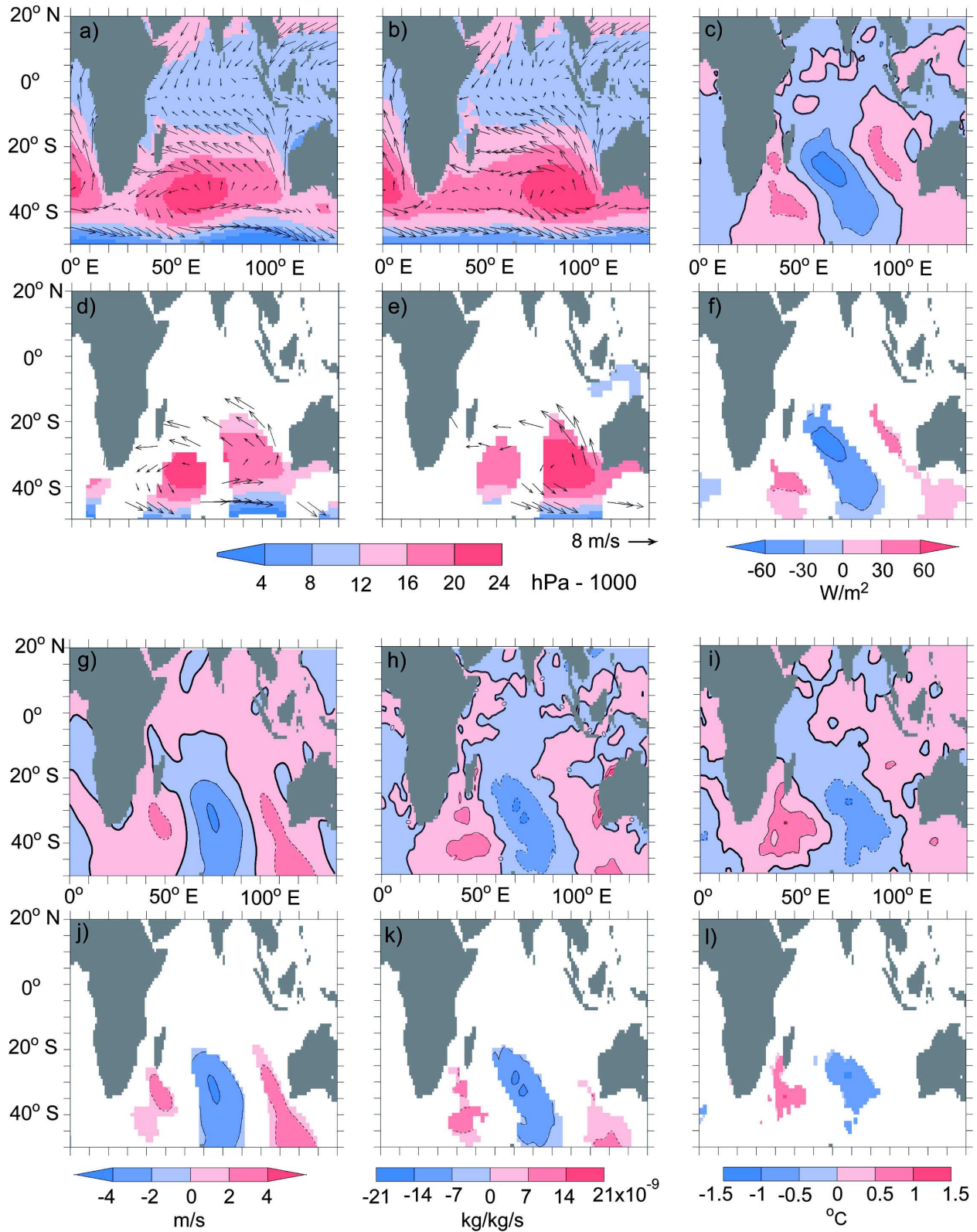


FIG. 7. (a) Mean SLP and wind composite during high western–low eastern SLP intervals. (b) As in (a), except for low western–high eastern SLP intervals. (c) Composite difference—high western minus high eastern SLP—of latent heat flux. (d)–(f) As in (a)–(c), respectively, except that only regions where the anomalies are significant at the 90% confidence level are shown. (g) Composite difference of southward wind. (h) Composite difference of $-\mathbf{V} \cdot \nabla_h q_a$. (i) Composite difference of SST anomalies. (j)–(l) As in (d)–(f), respectively, except that only regions where the anomalies are significant at the 90% confidence level are shown.

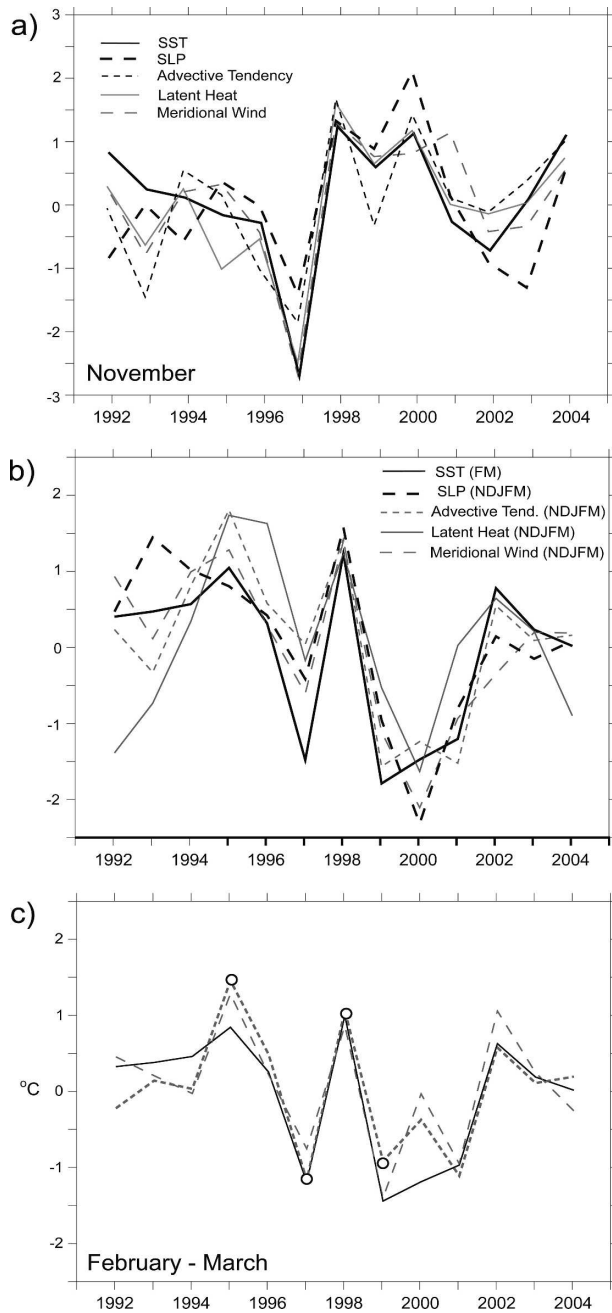


FIG. 8. (a) Southwestern to central basin differences of 30-day mean SST, SLP, advective water vapor tendency, latent heat flux, and meridional wind anomalies. The means are centered on 15 Nov for all variables except SST anomaly, which is centered on 30 Nov. Spatial averaging regions are listed in the text. These time series are normalized to have unit variance. Normalization factors are 1.0°C , 0.0041 Pa , $1.9 \times 10^8\text{ s}^{-1}$, 0.029 W m^{-2} , and 0.67 m s^{-1} , respectively. (b) Same indices as in (a), except that atmospheric variables are averaged from 1 Nov (of the year listed) to 30 Mar (year + 1) and SST is averaged from 1 Feb (year + 1) through 30 Mar (year + 1). Normalization factors are 1.2°C , 0.01 Pa , $3.6 \times 10^8\text{ s}^{-1}$, 0.09 W m^{-2} , and 0.93 m s^{-1} , respectively. (c) SST difference between the southwestern and central pole averaged over February and March. Spatial averaging regions are as defined in

of 2500 km and wind anomalies of several m s^{-1}) will cause first-order changes in Δq when acting over weekly or longer time scales.

Of course, changes in wind speed themselves cause changes in evaporation. To gain insight into the way in which wind speed and advection anomalies combine to produce a net effect on latent heat flux, we have devised a simple statistical model of the atmosphere. This boundary layer model may be pictured as a well-mixed column of air, of some fixed height h_a , in contact with the ocean and with the surrounding air masses. Tendencies in q_a are described by

$$\frac{\partial q_a(t)}{\partial t} = -Kq_a(t) + C[q_s - q_a(t)], \quad (8)$$

where $-Kq_a$ represents a generic removal of moisture. This may be due to either precipitation within the column or mixing/advection with surrounding air mass. Removal of moisture is necessary for the model to have a nonzero Δq in steady state. Here, K is assumed to remain constant and is specified such that $\overline{\Delta q}$ matches the climatological NCEP value (appendix B). A similar parameterization of the upper boundary condition was used by Seager et al. (1995). The second term on the right-hand side of this equation represents the exchange of water vapor with the ocean; C is derived from the standard latent heat flux parameterization (appendix B).

We assume the column starts in a steady-state flux condition with nonzero values of $\overline{\Delta q}$, $\overline{q_a}$, and \overline{S} and is exposed to a nonzero field $\nabla_h q_a$. We wish to find the latent heat flux anomaly caused by a step function perturbation in the low-level wind. This perturbation can initially change latent heat flux in two ways: it can change wind speed or it can advect $\nabla_h q_a$ and begin to change Δq . The wind speed anomaly created by a wind perturbation is

$$S' = [(\overline{U} + u')^2 + (\overline{V} + v')^2]^{(1/2)} - \overline{S}. \quad (9)$$

The new wind speed may be either larger or smaller than \overline{S} depending upon the direction of the perturbation wind, relative to the climatological wind vector. The advective trend is simply

$$A_a = -u' \frac{\partial \overline{q_a}}{\partial x} - v' \frac{\partial \overline{q_a}}{\partial y}. \quad (10)$$

←

this study (solid curve), as defined by Hermes and Reason (short dashed curve), and as defined by Behera and Yamagata (long dashed curve). Circles denote years that were cited as dipole years by Hermes and Reason, who considered data only up to year 1999.

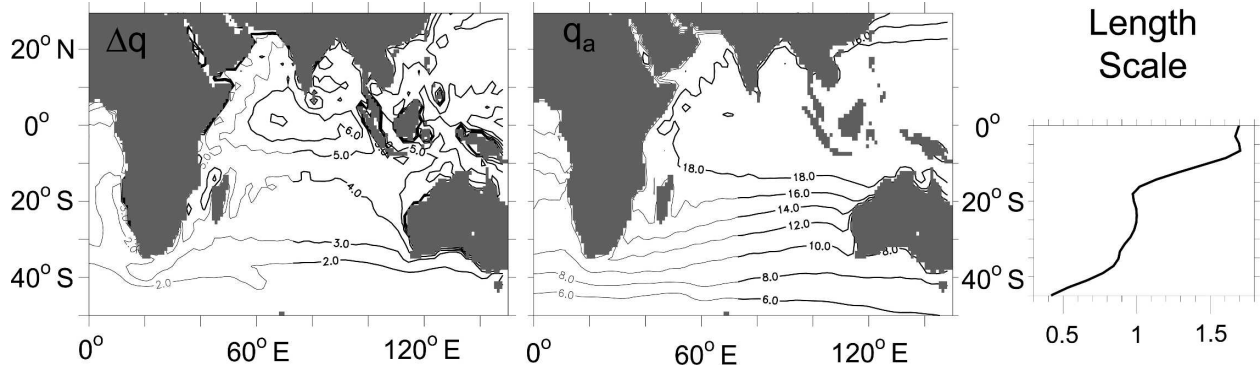


FIG. 9. (a) Annual mean Δq , 1992–2004. Contours are 1 g kg^{-1} . (b) As in (a), except for q_a . (c) $\text{Log}_{10}(l/100 \text{ km})$, where

$$l = \frac{\overline{\Delta q}}{|\partial q_a / \partial x + \partial q_a / \partial y|}.$$

Climatologically, air is undersaturated and heat is lost from the ocean by evaporation. Dry air advected to a moist climate would tend to increase Δq and increase evaporation. Moving moist air to a dry climate would do the opposite. Note that the same perturbation wind causes A_a and S' .

If the step function wind perturbation occurs at time $t = 0$, then for all $t > 0$

$$S = \bar{S} + S' \equiv S_2, \quad (11)$$

$$C = \frac{C_e \cdot S_2}{h_a} \equiv C_2, \quad (12)$$

and A_a appears as a term on the right-hand side of Eq. (8). As q_a evolves, it has a back effect on the air–sea exchange of water vapor at the surface. Thus, this system is an ordinary differential equation for $q_a(t)$, assuming that q_s , S_2 , and C_2 remain constant over the course of this perturbation. Strictly speaking, q_s does not remain constant, but its variability has little effect on the results discussed here (see appendix B).

The solution to Eq. (8), for $t_0 > 0$, with initial condition $q_a(0) = \bar{q}_a$ and S and C given by Eqs. (11) and (12), is

$$q_a(t_0) = \alpha e^{-(C_2 + K)t_0} + \beta, \quad (13)$$

with

$$\alpha = \bar{q}_a - \beta, \quad (14)$$

$$\beta = \frac{A_a + C_2 q_s}{K + C_2}, \quad (15)$$

and

$$q'_a = q_a(t_0) - \bar{q}_a \quad (16)$$

(see appendix B). We have chosen to use $t_0 = 7$ days, since this is near the decorrelation time scale of daily

mean atmospheric perturbations. Using longer time scales changes the result little since the e -folding time scale $[1/(C_2 + K)]$ is generally 2–6 days. The latent heat flux anomaly caused by (u', v') is

$$Q'_{\text{LH}} = C_e L_e \rho [S'(\overline{\Delta q} - q'_a) - \bar{S} \cdot q'_a], \quad (17)$$

which reduces to Eq. (2) when $S'q'_a$ is neglected. Trial and error has shown this to be a reasonable assumption in the cases considered here. This model, therefore, can be compared directly to the NCEP reanalysis data.

To evaluate the probability distribution of S' and $\Delta q'$ associated with this system, we have performed a Monte Carlo simulation of the effects of random wind perturbations on latent heat flux variability. At each location, climatological mean \bar{U} , \bar{V} , \bar{q}_a , $\overline{\Delta q}$ should, and $\nabla_h q_a$ values are specified from reanalysis data. Here, h_a is set at 1500 m. Five thousand pairs of zonal and meridional perturbation wind speeds are then applied to the model. The perturbation speeds are selected from a random normal distribution with zero mean and a standard deviation of 2 m s^{-1} . Wind direction is selected from a random distribution. The choice of wind perturbation distribution is somewhat arbitrary, although other types of random distributions (e.g., standard deviation of 3 m s^{-1} or choosing wind speed perturbations from a nonnormal distribution) yielded very similar results to those presented below. It was found that the use of 5000 pairs was enough to obtain a statistically stable response. A pair of S' and $\Delta q'$ anomalies was then found from the perturbation winds according to the equations above. To do this (u', v') were first plugged into Eqs. (9) and (10) to get S' and A_a and then these values, along with the climatological variables, are plugged into Eqs. (13) and (16) to yield $\Delta q'$. Note that this model is forced by perturbations selected from the same random distribution at each location, and thus,

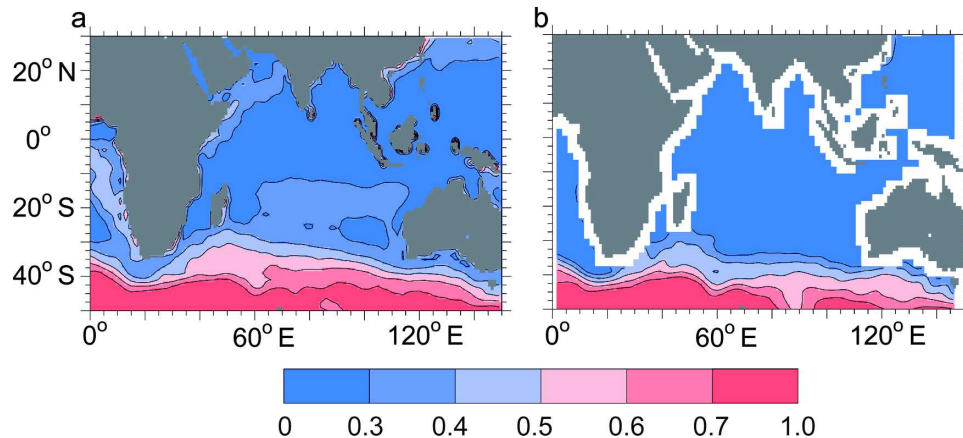


FIG. 10. Probability of $|R| > 1.5$ determined from (a) NCEP reanalysis and (b) atmospheric mixed layer model. Red indicates that latent heat flux anomalies are most often determined mainly by Δq .

any spatial trends apparent in the results must be caused by the climatological parameters (e.g., $\overline{\Delta q}$, $\overline{\nabla_h q_a}$, \overline{S} , \overline{U} , and \overline{V}).

First, we determined whether one can expect either $\Delta q'$ or S' to dominate the latent heat flux variability depending on location. To do this, the percentage of wind perturbations that caused $|R| > 1.5$ [see Eq. (3)] was tabulated at each location. The probability of this occurrence [$\text{Pr}(|R| > 1.5)$] shows a clear pattern of latitudinal variability (Fig. 10b). In the Tropics, $\text{Pr}(|R| > 1.5)$ indicates that S' is by far the larger determinant of latent heat flux variability. It also indicates that in the middle to high latitudes, latent heat flux variability is primarily determined by $\Delta q'$. The subtropics appear to be a transition between these two extremes, where both terms are important. This result can be partially understood by considering the latitudinal variation of \overline{S} and $\overline{\Delta Q}$ (see Fig. 9). Generally speaking, \overline{S} increases from the equator to the middle latitudes. This effectively reduces the magnitude of the latent heat flux anomaly associated with a given wind speed perturbation in the middle latitudes, relative to the Tropics. Also, $\overline{\Delta q}$ decreases with southward latitude, making Δq anomalies more important in the subtropics and middle latitudes than they are in the Tropics. The magnitude of $\overline{\nabla_h q_a}$ is also an important factor. In the Indian Ocean Tropics, $|\overline{\nabla_h q_a}|$ is small.³ Outside of the Tropics, there is a significant humidity gradient associated with the large SST gradient found throughout the subtropics and midlatitudes. Humidity advection becomes important here.

The general latitudinal trend seen in the model probability compares favorably to the trend found in re-

analysis data⁴ (Fig. 10a). Like the model, the reanalysis shows that $\Delta q'$ effects are dominant in the middle latitudes and that both S' and $\Delta q'$ are important in the subtropics. This comparison serves as partial confirmation that the processes included in the statistical model resemble those in the NCEP reanalysis. The model slightly under predicts the importance of Δq variability in the subtropics relative to NCEP, suggesting that the model gives a conservative estimate of the importance of Δq anomalies.

By what mechanism does the atmosphere create the 1998 and 1997 latent heat flux anomalies? We have already seen that both wind speed and Δq anomalies are important. The methodology used to create the statistical model may also be used to estimate the latent heat anomaly created by the observed wind anomalies. The model-estimated latent heat anomalies in these years (Figs. 11a,f) show qualitatively similar patterns to those observed in the reanalysis (cf. Fig. 5), although the magnitudes are somewhat underpredicted. What is most important to this discussion is that 1998 shows less latent heat loss in the southwest and more latent heat loss midbasin, similarly to the NCEP estimate. Likewise, the opposite pattern is shown in 1997. By altering the wind anomalies applied to the model, we can test which characteristics drive the latent flux variation. The latent heat anomaly that results when the zonal wind anomaly was set to zero (Figs. 11b,g) and when the net wind speed anomaly (Figs. 11c,h) was set to zero remains remarkably similar to the original (Figs. 11a,f).

³ This is not necessarily true in other basins. Near the Pacific cold tongue, for example, $\overline{\nabla_h q_a}$ reaches subtropical values.

⁴ For the reanalysis data, climatological monthly averages, interpolated to daily resolution, are used as the means. Deviations of the daily mean variables from this climatology are the anomalies.

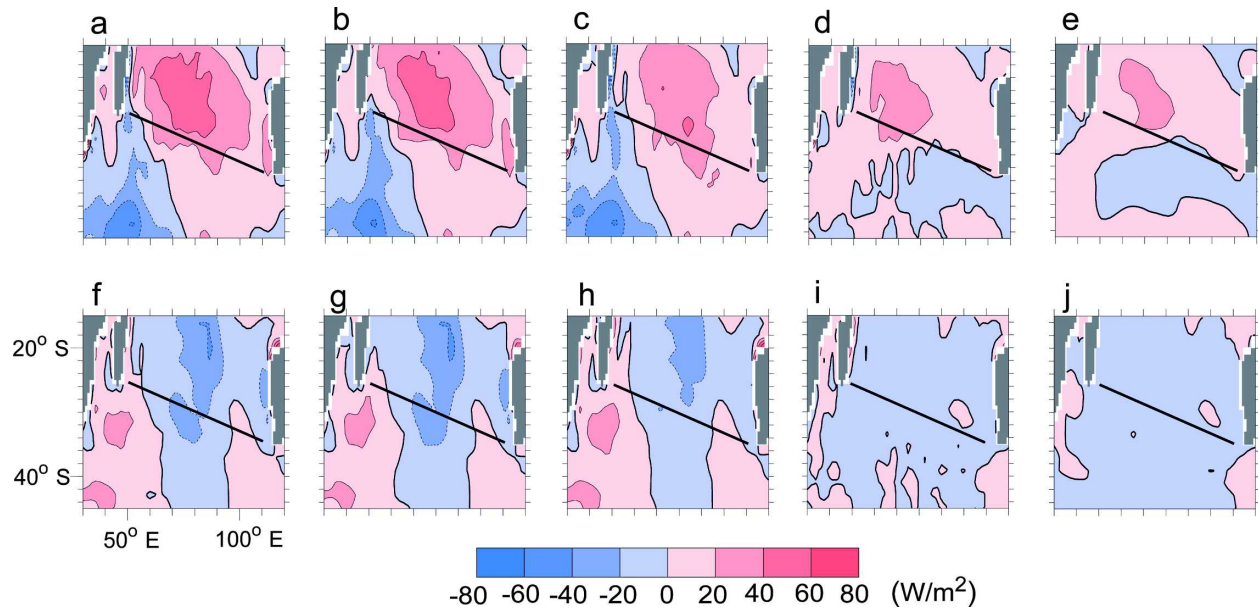


FIG. 11. The boundary layer model latent heat flux anomaly predicted from the November wind anomaly (a) 1997 and (f) 1998. (b), (g) As in (a), (f), except zonal wind anomalies are neglected. (c), (h) As in (a), (f), except wind speed anomalies are neglected. (d), (i) As in (a), (f), except that meridional wind anomalies are neglected. (e), (j) As in (a), (f), except humidity advection is neglected. The straight black line roughly marks the division between regions of observed anomalous warming and cooling (see Fig. 2).

This means that neither zonal wind nor wind speed perturbations are dominant causes of the modeled latent heat anomaly. If either humidity advection or the meridional wind anomaly is set to zero, however (Figs. 11d,i for meridional wind anomaly; Figs. 11e,j for humidity advection), there is a drastic reduction in the latent heat anomaly. This means that these model-estimated latent heat anomalies are driven by humidity anomalies that are caused, in turn, by anomalous humidity advection. It appears that the central basin anomaly is more affected by the absence of this advection process in 1998 than in 1997. This is consistent with the results from section 5, which indicated that the 1998 latent heat flux anomaly is almost wholly caused by humidity variability, whereas wind speed makes a significant contribution to the central basin anomaly of November 1997.

8. Summary and discussion

The mechanisms responsible for basin-scale summer subtropical Indian Ocean SST anomalies have been revisited here. Case studies suggest that latent heat flux variability is the primary and immediate cause, but that it is at least as important to consider the role of variability of Δq as of wind speed in order to understand the mechanism responsible [see Suzuki et al. (2004) for the case for wind speed variability]. Simple mixed layer model experiments indicate that the formation of thin summer ocean mixed layers is also important.

The role of Δq variability has not been carefully investigated previously. Here, it has been shown that the dependence of latent heat flux variability on wind speed and Δq anomalies tends to vary with latitude. Based on idealized atmospheric mixed layer model studies, Δq variability is important in driving subtropical and higher latitude latent heat flux variations. Case study atmospheric mixed layer experiments have also shown that Δq is of primary importance to the latent heat flux anomalies that drive the SST anomalies discussed here. This result is consistent with the analyses of NCEP reanalysis data presented here, which show that Δq variability is a crucial factor in driving the latent heat flux anomalies in each case considered.

Meridional advection of boundary layer humidity appears to be the primary source of the Δq variability of interest here. This direction is favored because the climatological near-surface horizontal humidity gradient tends to be meridional, being largely determined by SST, which has approximately zonal isotherms away from coasts. Based on typical climatological subtropical humidity gradients, meridional wind anomalies of several meters per second will cause first-order changes in Δq over a week or longer. A major finding of the work reported here is that meridional wind anomalies (rather than zonal wind anomalies, which have been the focus of previous investigations) are pivotal to the SST anomaly formation mechanism.

Wind speed variability can, however, sometimes play

an important role in driving the latent heat flux anomalies of interest. For example, off the east coast of Madagascar, wind speed variability accounted for about half of the latent heat flux anomaly in November 1997. Because climatological winds have a substantial northward component in this region, a southward wind anomaly will not only decrease wind speed but also will move moist air southward and decrease Δq . Thus, wind speed and humidity effects on latent heat flux tend to compliment each other in this region.

The meridional wind anomalies of interest appear to coincide with an extreme east or west location of the subtropical anticyclone. Anticyclones are prevalent features of near-surface subtropical atmospheric variability and efficiently transport dry air equatorward on their eastern flanks and moist air poleward on their western flanks.

The results shown here are consistent with the following SST anomaly formation mechanism. When the anticyclone is displaced to the western side of the basin, near Madagascar, the region directly south of Madagascar experiences relatively strong northerlies. These northerlies increase moisture advection to the region, which decreases Δq , which, in turn, decreases surface evaporation and eventually causes anomalously warm SST. In this position, the eastern side of the anticyclone advects drier midlatitude air to the central/eastern subtropics, cooling SST there by the opposite process. When the anticyclone is positioned near Australia (as in November 1997), the northerlies advect moist near-tropical air to the central rather than southwestern portion of the basin. Anomalous warming then occurs in the central part of the basin. With the anticyclone more distant, the area south of Madagascar no longer has a source of near-tropical moisture and the SST ends up cooler than normal.

Why are latent heat and SST anomaly patterns generally oriented from the northwest to the southeast? The answer lies in the meridional wind field associated with an anticyclone. Rather than being split along a meridian, such that all winds to the east of the center of the anticyclone are southerly and winds to the west of the center are northerly, as in a classical radially symmetric vortex, the meridional wind field associated with a subtropical anticyclone has a northwest to southeast orientation. In other words, winds in the north-by-northwest portion have a northward component and winds in the south-by-southeast portion have a southward component. The meridional wind anomalies that occur when the anticyclone migrates from one side of the basin to the other reflect this northwest to southeast orientation.

It is notable that previous studies concerned with

these same SST anomalies have examined the formation mechanism at coarser resolution, using seasonal or longer averages of SST and latent heat flux data (cf. Suzuki et al. 2004; Hermes and Reason 2005). Averaged over these longer time scales, the bimodal variability of the anticyclone described here is not readily apparent. Results show, however, that the mechanism discussed here is applicable to seasonal time scales.

The fact that the subtropical SST anomalies sometimes persist over several months and sometimes occur in conjunction with El Niño and La Niña events suggests that a coupled air–sea mechanism influences the location of the subtropical anticyclone. We cannot speculate on the details of this mechanism at this time but would like to encourage future studies to look at this important aspect of southern subtropical Indian Ocean variability.

Acknowledgments. The authors would like to acknowledge helpful suggestions from two anonymous reviewers and helpful conversations with N. A. Bond. This publication is partially funded by the Joint Institute for the Study of the Atmosphere and Ocean (JISAO) under NOAA Cooperative Agreement NA17RJ1232.

APPENDIX A

Comparing the Effects of $\Delta q'$ and S' on Q'_{LH}

The standard bulk latent heat flux parameterization (e.g., Large and Pond 1981) is

$$Q_{LH} = C_e L_e \rho S \Delta q. \quad (A1)$$

Although C_e and ρ are not technically constant, their variability is small compared to that of S and Δq and thus will be neglected.

A measure of the relative importance of S and Δq anomalies is found by first decomposing these variables into climatological monthly means (\bar{S} , $\bar{\Delta q}$) and deviations from these means (S' , $\Delta q'$):

$$S = \bar{S} + S' \quad \text{and} \quad (A2)$$

$$\Delta q = \bar{\Delta q} + \Delta q'. \quad (A3)$$

The standard bulk latent heat flux parameterization thus may be written as

$$Q_{LH} = C_e L_e \rho (\bar{S} \bar{\Delta q} + \bar{S} \Delta q' + \bar{\Delta q} S' + S' \Delta q'). \quad (A4)$$

Trial and error has shown that, in the cases presented herein, the fourth term on the right-hand side of Eq. (A4) may be neglected with little loss of accuracy, so that

$$\overline{Q_{LH}} \approx C_e L_e \rho \bar{S} \bar{\Delta q} \quad (A5)$$

and

$$Q'_{\text{LH}} \approx C_e L_e \rho (\bar{S} \Delta q' + \overline{\Delta q} S'). \quad (\text{A6})$$

After dividing Eq. (23) by Eq. (A5), it follows that

$$\frac{Q'_{\text{LH}} \Delta q'}{Q_{\text{LH}} \overline{\Delta q}} + \approx \frac{S'}{\bar{S}}. \quad (\text{A7})$$

APPENDIX B

Solving for $q_a(t)$

If K , A_a , C , and q_s are constant, the equation

$$\frac{\partial q_a}{\partial t} = -Kq_a + A_a + C(q_s - q_a) \quad (\text{B1})$$

is an ordinary differential equation for $q_a(t)$, with the general solution

$$q_a(t) = \alpha e^{-Ct} + \beta. \quad (\text{B2})$$

Here,

$$C = \frac{C_e S}{h_a} \quad (\text{B3})$$

and

$$K = \frac{C_e \bar{S} \bar{q}_a - \bar{q}_s}{h_a \bar{q}_a}. \quad (\text{B4})$$

The initial condition, $q_a(0) = \bar{q}_a$, yields

$$\bar{q}_a = \alpha + \beta. \quad (\text{B5})$$

By Eq. (B2), at $t = \infty$,

$$q_a(\infty) = \beta \quad (\text{B6})$$

and since $\partial q_a / \partial t = 0$ at $t = \infty$, Eq. (B1) yields

$$q_a(\infty) = \frac{A_a}{C_2 + K} + \frac{q_s C_2}{C_2 + K} = \beta. \quad (\text{B7})$$

Note that q_s would not actually remain constant after the wind perturbation is applied since the wind anomaly causes a latent heat anomaly that alters SST. Here, $\partial q_s / \partial T$ at $T \approx 20^\circ\text{--}25^\circ\text{C}$ is approximately $1 \text{ g kg}^{-1} \text{ }^\circ\text{C}^{-1}$. The Δq anomalies associated with the observed latent heat flux anomalies are on the order of 1 g kg^{-1} , so changes in SST of 1°C are significant. Strictly speaking, the expected variations in q_s are not small compared to this value. Including changes in q_s in this model, however, has relatively little effect on $\Delta q'$. This is because q_s appears in Eq. (B7), which means that changes in q_s drive similar changes in q_a . Since K is significantly smaller than C_2 (generally less than 30%), the changes in q_s caused by anomalous heating of the

surface force similar changes in q_a . Changes in SST are, therefore, of secondary importance to $\Delta q'$.

REFERENCES

- Alexander, M. A., I. Bladé, M. Newman, J. R. Lanzante, N.-C. Lau, and J. D. Scott, 2002: The atmospheric bridge: The influence of ENSO teleconnections on air–sea interaction over the global oceans. *J. Climate*, **15**, 2205–2231.
- Behera, S. K., and T. Yamagata, 2001: Subtropical SST dipole events in the southern Indian Ocean. *Geophys. Res. Lett.*, **28**, 327–330.
- , P. S. Salvekar, and T. Yamagata, 2000: Simulation of interannual SST variability in the tropical Indian Ocean. *J. Climate*, **13**, 3487–3499.
- Carton, J. A., X. Cao, B. S. Giese, and A. M. Da Silva, 1996: Decadal and interannual SST variability in the tropical Atlantic. *J. Phys. Oceanogr.*, **26**, 1165–1175.
- , G. Chepurin, X. Cao, and B. S. Giese, 2000: A simple ocean data assimilation analysis of the global upper ocean 1950–1995. Part I: Methodology. *J. Phys. Oceanogr.*, **30**, 294–309.
- England, M. H., C. C. Ummerhofer, and A. Santoso, 2006: Interannual rainfall extremes over southwest Western Australia linked to Indian Ocean climate variability. *J. Climate*, **19**, 1948–1969.
- Fauchereau, N., S. Tzaska, Y. Richard, P. Roucou, and P. Camberlin, 2003: Sea-surface temperature co-variability in the southern Atlantic and Indian Oceans and its connections with the atmospheric circulation in the southern hemisphere. *Int. J. Climatol.*, **23**, 663–677.
- Goddard, L., and N. E. Graham, 1999: Importance of the Indian Ocean for simulating rainfall anomalies over eastern and southern Africa. *J. Geophys. Res.*, **104**, 19 099–19 116.
- Hermes, J. C., and C. J. C. Reason, 2005: Ocean model diagnosis if interannual coevolving SST variability in the southern Indian and south Atlantic Oceans. *J. Climate*, **18**, 2864–2882.
- Huang, B., and J. L. Kinter, 2002: Interannual variability in the tropical Indian Ocean. *J. Geophys. Res.*, **107**, 3199, doi:10.1029/2001JC001278.
- Kalnay, E., and Coauthors, 1996: The NCEP/NCAR 40-Year Reanalysis Project. *Bull. Amer. Meteor. Soc.*, **77**, 437–471.
- Large, W. G., and S. Pond, 1981: Open ocean momentum flux measurements in moderate to strong winds. *J. Phys. Oceanogr.*, **11**, 324–336.
- Levitus, S., 1994: World Ocean Atlas 1994 CD Rom Sets. National Oceanographic Data Center Informal Rep. 13, 30 pp.
- Mason, S. J., and M. R. Jury, 1997: Climatic variability and change over southern Africa: A reflection on underlying processes. *Prog. Phys. Geogr.*, **21**, 23–50.
- Nicholson, S. E., 1997: An analysis of the ENSO signal in the tropical Atlantic and western Indian Oceans. *Int. J. Climatol.*, **17**, 345–375.
- Paulson, C. A., and J. J. Simpson, 1977: Irradiance measurements in the upper ocean. *J. Phys. Oceanogr.*, **7**, 952–956.
- Price, J. F., R. A. Weller, and R. Pinkel, 1986: Diurnal cycling: Observations on models of the upper ocean response to diurnal heating, cooling and wind mixing. *J. Geophys. Res.*, **91** (C7), 8411–8427.
- Reason, C. J. C., 1999: Interannual warm and cool events in the subtropical mid-latitude south Indian Ocean region. *Geophys. Res. Lett.*, **26**, 215–218.
- , 2001: Subtropical Indian Ocean SST dipole events and southern African rainfall. *Geophys. Res. Lett.*, **28**, 215–218.

- , and H. Mulenga, 1999: Relationships between South African rainfall and SST anomalies in the southwest Indian Ocean. *Int. J. Climatol.*, **19**, 1651–1673.
- Reynolds, R. W., N. A. Rayner, T. M. Smith, D. C. Stokes, and W. Wang, 2002: An improved in situ and satellite SST analysis for climate. *J. Climate*, **15**, 1609–1625.
- Rocha, A., and I. Simmonds, 1997a: Interannual variability of south-eastern African summer rainfall. Part 1: Relationships with air-sea interaction processes. *Int. J. Climatol.*, **17**, 235–265.
- , and —, 1997b: Interannual variability of south-eastern African summer rainfall. Part 2: Modelling the impact of sea-surface temperatures in rainfall and circulation. *Int. J. Climatol.*, **17**, 267–290.
- Saji, N. H., and T. Yamagata, 2003: Structure of SST and surface wind variability during Indian Ocean dipole mode events: COADS observations. *J. Climate*, **16**, 2735–2751.
- Seager, R., Y. Kushnir, and M. A. Cane, 1995: On the heat flux boundary conditions for ocean models. *J. Phys. Oceanogr.*, **25**, 3219–3230.
- Smith, S. R., D. M. Legler, and K. V. Verzone, 2001: Quantifying uncertainties in NCEP reanalyses using high-quality research vessel observations. *J. Climate*, **14**, 4062–4072.
- Suzuki, R., S. K. Behera, S. Iizuka, and T. Yamagata, 2004: Indian Ocean subtropical dipole simulated using a coupled general circulation model. *J. Geophys. Res.*, **109**, C09001, doi:10.1029/2003JC001974.
- Walker, N. D., 1990: Links between South African summer rainfall and temperature variability of the Agulhas and Benguela current systems. *J. Geophys. Res.*, **95**, 3297–3319.
- Xie, S.-P., H. Annamalai, F. A. Schott, and J. P. McCreary, 2002: Structure and mechanisms of South Indian Ocean climate variability. *J. Climate*, **15**, 864–878.
- Yu, L., and M. M. Rienecker, 1999: Mechanisms for the Indian Ocean warming during the 1997–98 El Niño. *Geophys. Res. Lett.*, **26**, 735–738.